actuators

MDPI

Article

Tug-of-War-Style High-Force Fluidic Actuation for Small Diameter Steerable Instruments

Robert Lathrop [1,*], Mouloud Ourak [1], Jan Deprest [2] and Emmanuel Vander Poorten [1]

[1] Mechanical Engineering Department, KU Leuven, Celestijnenlaan 300B, 3001 Leuven, Belgium; mouloud.ourak@kuleuven.be (M.O.); emmanuel.vanderpoorten@kuleuven.be (E.V.P.)
[2] Department of Obstetrics and Gynecology, UZ Leuven, Herestraat 49, 3000 Leuven, Belgium; jan.deprest@uzleuven.be
* Correspondence: bob.lathrop@kuleuven.be

Abstract: Miniature steerable instruments have the potential to reduce the invasiveness of therapeutic interventions and enable new treatment options. Traditional ways of driving such instruments rely on extrinsic systems due to the challenge of miniaturizing and embedding intrinsic actuators that are powerful enough near the instrument tip or within the instrument shaft. This work introduces a method to amplify the output force of fluidic actuators by connecting their outputs in parallel but distributing them serially in currently underutilized space along the device's long axis. It is shown that this new approach makes it possible to realize a significant force amplification within the same instrument diameter, producing a 380% higher static force and a further driving motion of the steerable bending segment 55.6° than an actuator representing the current state of the art, all while occupying a similar footprint.

Keywords: actuators; soft robotics; steerable surgical devices

check for updates

Citation: Lathrop, R.; Ourak, M.; Deprest, J.; Poorten, E.V. Tug-of-War-Style High-Force Fluidic Actuation for Small Diameter Steerable Instruments. *Actuators* **2024**, *13*, 444. https://doi.org/10.3390/act13110444

Academic Editor: Luigi de Luca

Received: 10 September 2024
Revised: 18 October 2024
Accepted: 5 November 2024
Published: 7 November 2024

1. Introduction

Recent advances in the development of medical robotic systems have played a significant role in enabling new, minimally invasive surgical (MIS) procedures, improving patient outcomes and providing surgeons with a wider array of problem-solving tools [1,2]. To build upon this progress, it is important to develop new steerable MIS devices that can be navigated within the patient to access and treat anatomically remote surgical sites. Such steerable MIS devices have been developed for use in a wide range of medical fields including cardiology, endoscopy, and neurology, among many others [3–7]. These tools enable surgical access for diagnostic procedures that evaluate tissue health through means such as direct visualization, biopsy, intravenous ultrasound, and optical coherence tomography [8,9], as well as enabling therapeutic procedures such as laser ablation, the implantation of stents, and the removal of pathologic tissues or vascular obstructions [10,11].

Common challenges in the design of these tools and the systems used for their actuation include trade-offs between a device's flexibility, rigidity, durability, ability to fit through narrow anatomic openings, and ability to respond quickly to user input and its range of motion (ROM) and number of controllable degrees of freedom (DOF) [12]. Most steerable MIS devices can be classified as either extrinsically or intrinsically actuated. Extrinsically actuated systems use actuators placed relatively far from the surgical site, proximal to the operator, to generate controlled distal movement at the tip of the device. The proximal motion is hereto transferred via a transmission system through the device to the end effector. Intrinsically actuated devices contain embedded actuators that act at or very near to the surgical field, with little to no additional mechanical transmission [12].

Typical examples of extrinsically actuated steerable surgical devices are cable-driven systems, such as in the rigid or flexible instruments of the Da Vinci robots by Intuitive Surgical Inc. (Sunnyvale, CA, USA), or concentric tube robotic systems, which rely on

tubes to transmit motion and employ external actuators to drive the relative motion of pre-bent tubes, producing steerable movement [13]. While extrinsically actuated systems have proven useful for a wide array of surgical procedures, there are several opportunities to improve on the capabilities they offer. Hand-held surgical instruments with external driving systems add significant weight and bulk in comparison to the manual surgical tools that surgeons are accustomed to. This limits the tactile feel that surgeons experience while using the tools and can limit the clinical adoption of new robotic devices due to the need for retraining and modifying existing technique. Extrinsically driven systems also typically have limited range of access within the patient, as it is often difficult to transmit actuation forces through tortuous paths in the anatomy without exerting unintended forces on the surrounding tissues. External drive systems can also be very large and costly pieces of capital equipment, limiting their use to affluent healthcare systems that can afford the additional cost and inconveniencing staff that must navigate around the system in the operating room [12].

Intrinsically actuated surgical devices have been developed to address these limitations. These devices use small, lightweight actuators to produce motion and apply forces near to the actuation target. Intrinsic actuation can also reduce the challenge of steering MIS devices to surgical sites that are deep within the patient's body or must be accessed via a tortuous path by removing the need to transmit driving forces through the length of the device while maintaining flexibility as it is advanced into the body. The need to account for parasitic forces produced by transmission cables routed through the device is also removed, and there is increased potential for miniaturization of multi-DOF devices due to the elimination of separate transmission mechanisms for each mode of actuation [14]. Intrinsically actuated MIS devices have been developed using technologies such as shape memory alloys [15], magnetics [16], and fluidic actuators [17]. Pneumatic artificial muscles (PAMs) are a subset of fluidic actuators that are particularly promising for use in miniature steerable instruments, as elaborated upon in Section 1. While PAMs possess a laudable power–volume ratio, the limited space available within MIS devices (especially in terms of the constraints on the allowable diameter) does impose a limit on the achievable output force using intrinsic fluidic actuation. A PAM-actuated flexible fetoscope was recently developed for fetoscopic laser coagulation which used a handpiece-embedded actuator to steer the movement of a fetoscope tip, enabling fetal surgeons to more easily target tissues for coagulation without putting excessive strain on the maternal or fetal tissues [18], as shown in Figure 1. The shaft of this device was total of 30 cm in length, with a flexible length of 3 cm at the tip. This device required significant actuation force due to the need to bend an inflexible laser fiber to a high angle over a small bending radius. It is advantageous for the device to bend the laser fiber to a high angle over the smallest possible radius, as this reduces movement of the surgeon's endoscopic camera field of view (FOV) and the variation in distance between device tip and tissue surface while the device is steered. Minimizing changes in distance between device and tissue is particularly important for laser coagulation procedures, as any variation can lead to over or under treatment of the target tissues.

The previously developed steerable fetoscope was limited in terms of achievable bend angle at small bend radii due to spacial limitations in the device handpiece, which prevented the use of a larger-diameter, higher-force PAM. In this paper, a new "tug-of-war"-style collaborative fluidic actuation scheme is introduced and evaluated. This design uses multiple PAMs distributed along the axis of a device with their proximal and distal connection points attached such that each contributes additional force to the actuation target, while remaining small enough in diameter to fit within the footprint of typical fetoscopes currently used for laser ablation procedures. A prototype is constructed and its force and stroke output capabilities are evaluated. The prototype is then used to bend a laser fiber at smaller bend radii than achievable with the previously introduced device, demonstrating its potential for producing more capable intrinsically actuated semi-rigid surgical devices.

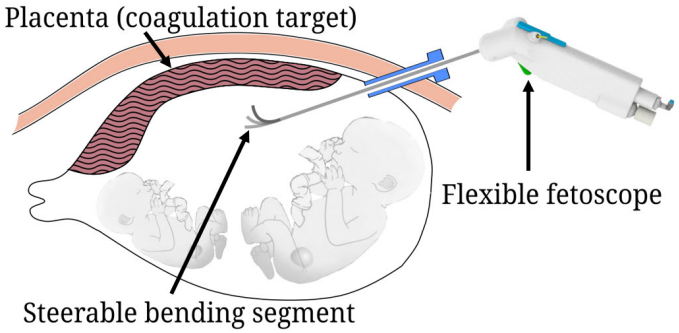

Figure 1. An intrinsically actuated flexible fetoscope being steered to access difficult-to-reach points on the placental surface for a laser coagulation procedure.

Technical Background

Pneumatic artificial muscles have been developed for use in a wide range of applications including soft robotics, healthcare, aerospace, and industrial robotics [19–21]. PAMs are often selected for use due to their high power-to-weight ratio, fast response bandwidth, simple construction, and inherent compliance. They have also shown significant potential for miniaturization, having been made as small as 1 mm in diameter [22]. These actuators are composed of a flexible pneumatic bladder wrapped in an inelastic braided mesh which is held in place by end connectors on either side and provided with a pneumatic air supply. During actuation, pressure is applied to inflate the bladder, causing it to expand radially and contract axially, thereby transmitting force to the end connectors via the braided mesh. This functional principle is illustrated in Figure 2a.

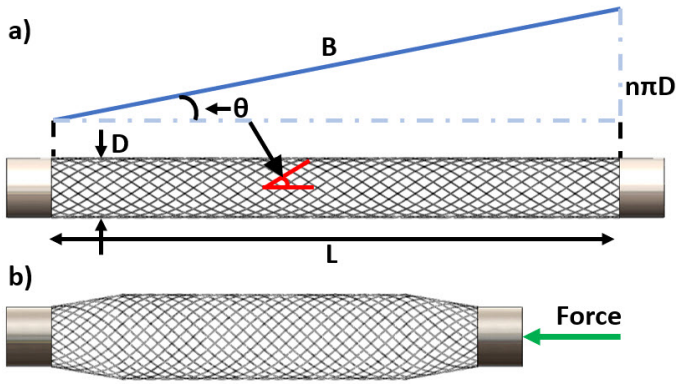

Figure 2. Basic functional principle and geometry of a pneumatic artificial muscle, including (**a**) PAM at rest with labeled geometric parameters relating the braid geometry to actuator dimensions and (**b**) pressurized PAM contracting axially and exerting an actuation force.

A common model used to predict the static force generation of a PAM is the Gaylord model [23], which takes the form of Equation (1). The geometric parameters of a PAM that determine its actuation capabilities are shown in Figure 2b, from which the relationships in Equations (2) and (3) are developed. Substituting Equations (2) and (3) into Equation (1) produces Equation (4), the predicted PAM blocked force output in terms of PAM braid angle and diameter.

$$F = \frac{P}{4n^2\pi}(3L^2 - B^2) \tag{1}$$

$$L = B\cos(\theta) \tag{2}$$

$$D = \frac{B\,sin(\theta)}{n\,\pi} \tag{3}$$

$$F = \frac{P\,\pi\,D^2}{4\,sin^2\,\theta}(3\,cos^2(\theta) - 1) \tag{4}$$

where:

F = Force
P = Actuation pressure
n = # of turns a braid strand makes along PAM length
L = PAM Length
B = Length of a single braid strand
θ = Angle between a braid strand and long axis of PAM
D = PAM Diameter

It is important to note that the force predicted by (4) is a function of the actuator's cross-sectional area but not of its length. To increase the output force of a typical PAM, one must either change the braid geometry, increase its diameter, or—as is proposed in this work—connect the outputs of multiple actuators in parallel. A long PAM will provide additional stroke length in comparison to short PAMs, but no theoretical change in maximum blocked force output (though force output as a function of absolute device contraction length will vary).

An important concern when designing PAMs for intrinsic actuation is the maximum size that a pressurized muscle will occupy. It is possible to estimate the maximum diameter and change in length that a PAM will achieve during actuation using Equations (2) and (3). To estimate the size of the fully actuated PAM, one must first find the maximum braid angle that the muscle will reach during actuation. This angle can be calculated by solving (4) with an output force of zero, representing the case where a PAM is able to contract freely through its full range of motion until its movement is naturally constricted by the geometry of the braid. Taking this approach results in an angle of 54.7°, which can be used in Equations (2) and (3) to determine the theoretical maximum diameter and contraction length for a PAM of a particular geometry. It is important to note that these predicted values will be higher than can be achieved by a real PAM. This is due to simplifying assumptions made during the formulation of the Gaylord model, which does not account for limiting factors such as the necessary elastic deformation of the PAM bladder or friction between the braid strands. Still, this method is useful for obtaining an estimation of the maximum PAM dimensions when actuated, ensuring adequate space is allocated within constrained environments such as the lumen of a steerable MIS device.

A novel actuator design is proposed which links the proximal and distal ends of a series of PAMs as shown in Figure 3. This creates a series of points which alternate between being fixed to the base of the device and coupled to the actuation target (in the case of a laser ablation fetoscope, the tip of the flexible bending segment). In this configuration, the PAMs are placed serially along the length of the actuator but connected such that their outputs act in parallel, allowing each PAM to contribute to the total actuation force much as team members participating in a sort of "tug-of-war" against the actuation target. This benefit comes at the cost of taking up additional space along the device axis (an abundantly available resource in long, thin steerable MIS devices) and producing a shorter stroke length than a single PAM of equivalent length. The pneumatic supply is shared between PAMs acting on a common actuation target to reduce the number of supply tubes routed through the device. This design can be extended for an arbitrary number of collaborative PAMs, opening interesting possibilities for the development of small-diameter actuators capable of delivering very high forces. There is significant potential for this design to enable the development of new intrinsically actuated surgical devices which benefit from high driving force and have small stroke length requirements such as graspers, dissectors, and low bend-radius steerable tools.

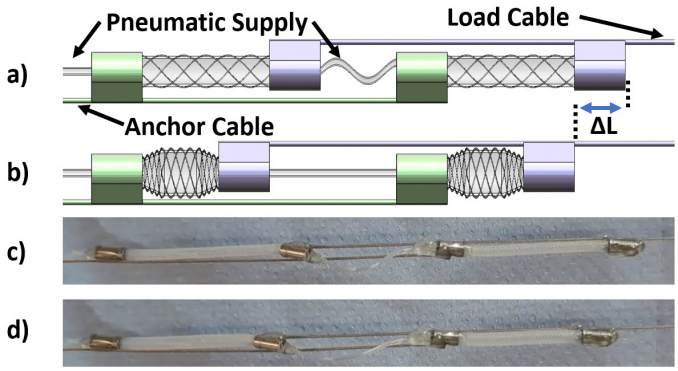

Figure 3. Serially linked PAMs (**a**) at rest and (**b**) contracting during actuation. Proximal PAM ends are connected and fixed in place via a cable (green). Distal PAM ends are connected to the actuation target via a second cable (blue). An assembled prototype chain of linked PAMs are shown (**c**) at rest and (**d**) during actuation.

2. Methods and Materials

To evaluate the performance of the proposed design, two prototype actuators were constructed: one using a group of collaboratively connected PAMs and a second with a single PAM of equivalent length to the sum of the collaborative PAMs. A total actuator length of 250 mm was selected to fit within the 300 mm shaft length of currently available fetoscopic devices used for laser ablation procedures and a previously developed flexible fetoscope [18]. For the collaborative group, the 250 mm actuator length was split evenly between 5 PAMs of equal length. This number was selected in order to ensure that the actuator would be capable of providing useful forces at stroke lengths up to 5 mm, 10% of the resting length of each PAM, to actuate the device bending segment through its maximum range of motion. Subdividing the actuator length further (building 6 or more collaborative PAMs and keeping the overall actuatable length constant) would produce higher forces at short stroke lengths, but the force output as a function of contraction length will decrease more quickly as the resting length of the PAMs is reduced. The chosen materials were selected to produce PAMs with a theoretical maximum actuated diameter of 2.8 mm using the method described in Section 1. For a flexible fetoscope containing a 1.1 mm OD laser fiber channel and max 1 mm diameter chip-on-tip and LED illumination wire bundle, this actuator configuration would be usable without interfering with other components in a device with a footprint as small as 3.9 mm in diameter, comparable in size to the current clinical state of the art. Prototype PAMs were constructed using the following components:

- **End Connectors** : Stainless steel tubing (2.2 mm OD, Salomon's Metalen, Groningen, the Netherlands)
- **Pneumatic bladder**: 50A durometer silastic silicone tubing (2.0 mm OD, Dow Corning, Midland, MI, USA). Material selected for its flexibility and elasticity, to safely contain the actuation pressure and inflate to engage the braided mesh.
- **Braided mesh**: 0.07 mm diameter polyamide strands woven into 1.5 mm OD diameter mesh (Bossert Kast, Pforzheim, Germany). Material selected for its low friction and inextensibility (elastic modulus 2.7 GPa), to efficiently transfer force from bladder to end connectors.
- **Pneumatic supply**: PTFE tubing (0.64 mm OD, Scientific Commodities, Lake Havasu City, AZ, USA)
- **Transmission cable**: Stainless steel (0.27 mm Diameter, CarlStahl, Süssen, Germany)
- **Adhesive and sealant**: 204-CTH-F UV Adhesive (Dymax, Torrington, CT, USA)

The PAMs were assembled by placing sections of pneumatic bladder within the braided mesh and then inserting the ends of a pneumatic supply tube and steel transmission cable to the bladder lumen before sealing into the end connectors with UV adhesive. Each collaborative PAM was built with a cable extending from each end connector in order to enable connection to the fixed end and actuating ends on the adjacent actuators. The PAMs

were then joined progressively, with the cable at the completed end of the chain held in a vice and the in-progress end brought to a neutral tension while the cables of successive PAMs are fixed to the connectors of their neighbors, maintaining a straight alignment of the flexible components while minimizing any variable pre-tensioning of the individual PAM segments. To ensure balanced actuation between the PAMs, dimensions of the braid, tubing, end connectors, and lengths of cable between PAMs were carefully controlled throughout assembly. The final actuatable lengths of the assembled collaborative PAMs were measured to be between 49.3 and 50.2 mm, within 2% of the targeted length. The single PAM was measured to be 249.5 mm in length. Each actuator configuration was driven using a single pressure source, with the five collaborative PAMs pneumatically connected in series as shown in Figure 3.

When building a series of linked PAMs, it is important to use connecting pieces which will not impede the natural motion of the muscles during their actuation. For the pneumatic supply tubes shown in Figure 3, flexible materials that could accommodate the motion of the PAM ends are generally undesirable as they are likely to inflate under pressurization. It is best to leave enough slack between one PAM's distal end connection and the next PAM's proximal connection in order to prevent the pneumatic supply line from impeding actuator movement. Care should also be taken to minimize interference between the cables and the PAM's outer surfaces at full pressurization, as this could lead to wear to the PAM braid and bladder over repeated cycling.

If large chains of actuators are linked together, there should eventually be a noticeable effect on dynamic performance as pressure levels propagate from the control valve through each muscle until they reach the last. This limitation is important for future evaluation, but is not observed to a significant extent in the prototypes built for this study. Fluid pressure transmission, available axial length, and material strength of the components are the only theoretical limiting factors on the output force achievable using this design.

A custom test stand, shown in Figure 4, was used to evaluate actuator performance. This stand consists of a Tedea–Huntleigh (Columbus, NE, USA) model 1022 10 kg load cell, a Baumer (Frauenfeld, Switzerland) model OADM 12I6460/S35A laser distance sensor, a FESTO (Esslingen, Germany) model VEAA proportional pressure regulator, and a Keller (Winterthur, Switzerland) model PA-21Y pressure sensor, along with fixturing elements to rigidly attach muscles to the baseplate and linear slides. All data acquisition and control was done via a custom LabVIEW program using a National Instruments (Austin, TX, USA) CDAQ-9174 system with appropriate analog I/O modules for interfacing with the sensors and valve.

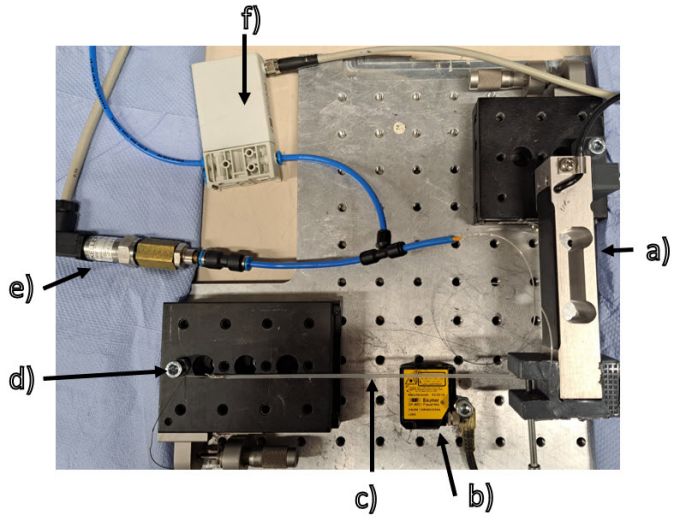

Figure 4. Test set-up for force and displacement measurements including (**a**) force sensor, (**b**) laser distance sensor, (**c**) pneumatic artificial muscle clamped in place for evaluation, (**d**) lockable linear slide, (**e**) pressure sensor, and (**f**) pressure control valve.

3. Experiments

The actuation capabilities of each prototype were tested using the jig shown in Figure 4. Maximum blocked force was evaluated by clamping the prototypes into place in the fixture and locking the linear slide in place, preventing any motion. Each prototype was then actuated three times by a sinusoidal pressure input at 0.1, 0.5, 1.0, and 1.5 Hz to evaluate its range of frequency response; 0.1 Hz was selected as the lowest frequency because actuator performance at lower frequencies was found to be not significantly different, while 1.5 Hz was selected to demonstrate a worst-case response to an actuation frequency significantly higher than expected for use in most MIS instrument applications. The results of this testing are shown in Figure 5a. The collaborative PAM chain produced a maximum output force of 26.1 N, while the single PAM produced only 6.8 N. Both prototypes displayed a significant increase in hysteresis and a reduction in force output as frequency increased, with the collaborative prototype reaching 18.3 N or only 70.1% of the maximal output force and the single PAM reaching 6 N or only 88.2% of the maximal output force at 1.5 Hz. This difference in maximum achieved force may be a function of the limitations of the pneumatic throughput of the selected valve. The larger drop in performance of the collaborative PAMs merits further investigation but may be influenced by the rate of pressure propagation through the muscles or deformation of the additional lengths of cable needed to connect their ends.

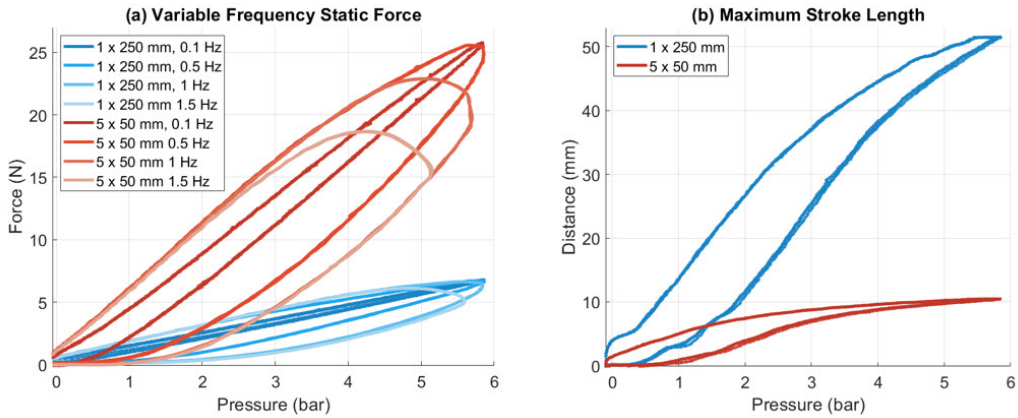

Figure 5. Results of comparative characterization testing for a single PAM and a group of 5 collaborative PAMs, including (**a**) maximum static force generation at variable frequency pressure actuation and (**b**) maximum stroke length when free to contract.

To assess the stroke length of each prototype, the linear slide in Figure 4 was released in a second test. The PAMs could then contract freely on pressurization, only resisted by a soft spring. As shown in Figure 5b, the maximum stroke was 10.5 mm for the collaborative PAMs whereas it was 51.5 mm for the single PAM. The collaborative PAMs displayed an increased deadband pressure and hysteresis, likely due to slight differences in bladder length and pretension among its sub-unit PAMs. This may explain a variation in pressure upon which the muscles start to engage.

After establishing the baseline functionality of the prototypes, the ability to bend a stiff 1 mm-diameter laser fiber that is typically used in fetoscopic laser coagulation procedures was assessed. A 15 mm-long bending segment was constructed using two flexible 1.3 mm-diameter braid-reinforced PTFE tubes fixed into 3.3 mm-diameter stainless steel end connectors. One tube served as a working channel for the laser fiber, while the other contained the attachment cable to the actuator, as shown in Figure 6a. This assembly was then enclosed in a heat-shrunk PTFE sheathe to maintain coherence during actuation.

The laser fiber is able to translate freely back and forth through the segment. This test condition is important, as in the real intervention surgeons need to be able to adjust the length of the portion of the fiber that extrudes from the working channel of the device at

any time. This is important for establishing the distance to the ablation surface but also helps them understand the orientation of the camera and fetoscope.

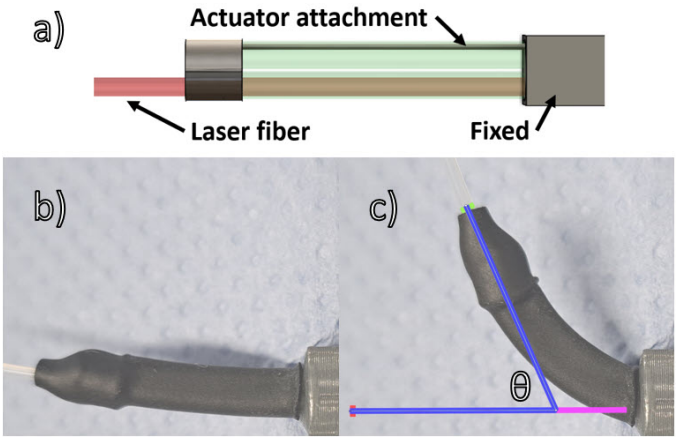

Figure 6. Comparative images of (**a**) the internal construction of the bending segment, (**b**) the maximum bend angle achieved for the 15 mm-long steerable bending segment actuated by a single 250 mm-long PAM, and (**c**) the same segment actuated by the collaborative output of 5 × 50 mm-long PAMs, showing the measured angle of the bent laser fiber relative to its unactuated position.

Each prototype was connected to the driving cables and actuated across its full range of motion, with the resultant bend angle measured by image analysis using the software ImageJ, U. S. National Institutes of Health, Bethesda, MD, USA, version 1.54f. While fixing each actuator in place for testing, its pre-tension was adjusted to the minimum amount required to remove slack from the driving cables. Pre-tension was minimized for this study, as significant pre-tensioning can deflect the neutral tip position of flexible MIS devices. This resulted in a baseline tension of 0.48 N for the collaborative actuator and 0.14 N for the single PAM, with the collaborative actuator requiring a slightly higher tension to counteract the additional weight of its transmission cables. Pictures were taken using a camera centered above the fixed end of the bending segment in order to ensure consistent perspective and position. Bend angle was defined as shown in Figure 6c, by finding the intersection of the laser fiber's unactuated position and the line tangent to the laser fiber's axis when bent. Tests were repeated five times by removing and re-applying the target pressure, with average achieved bend angle ± standard deviation reported in Table 1 and displayed in Figure 7. The collaborative PAMs produced a significantly higher average bend angle at 65.9° compared to the single PAM's 10.2° and did so while occupying a similar footprint. To assess stability over repeated actuation, the bend angle produced at maximum pressurization was re-measured after applying 100 cycles of a sinusoidal pressure input with 6 bar amplitude at 0.5 Hz frequency, with results reported in Table 1. A small decrease in bend angle is observed after repeated cycling, likely due to relaxation of the actuators and transmission cables. This could be addressed in future designs by applying a controlled stretching regimen to the actuators before they are installed, thereby inducing any potential relaxation before the actuators are pre-tensioned.

Another test was performed to establish the diameter of the collaborative PAM as a function of its pressurization, an important consideration when designing for the limited cross-sectional space available in a steerable MIS device. The chain of actuators was attached to the bending segment, constrained in the test jig shown in Figure 4. Continuous measurement of the movement of the outer surface by a laser distance sensor was attempted but was not able to produce consistent measurements due to the irregular surface of the moving braid and optically translucent silicone tubing used as a bladder. Instead, the prototype was pressurized from 0 to 6 bar in 1-bar increments, with its diameter measured manually via a caliper at each step. The results of this test are reported in Table 1, showing

slow initial expansion at low pressures followed by approximately linear increase up to a maximum of 2.62 mm.

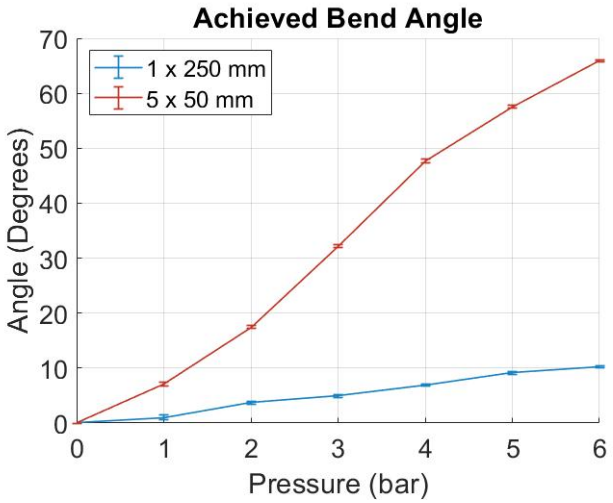

Figure 7. Bend angles achieved by actuation using a single 250 mm-long PAM compared to the collaborative output of five 50 mm PAMs.

Table 1. Bend angle and diameter measurement results; all values are the average ± standard deviation over five repeated tests.

Actuator	Pressure (bar)	Bend Angle (Degrees)	Diameter (mm)
Single	0	0.0 ± 0.0	
Single	1	1.0 ± 0.3	
Single	2	3.7 ± 0.3	
Single	3	5.0 ± 0.3	
Single	4	6.9 ± 0.2	
Single	5	9.1 ± 0.3	
Single	6	10.2 ± 0.2	
Single [1]	6	9.5 ± 0.2	
Collaborative	0	0.0 ± 0.0	2.07 ± 0.01
Collaborative	1	7.1 ± 0.3	2.11 ± 0.03
Collaborative	2	17.5 ± 0.2	2.16 ± 0.01
Collaborative	3	32.2 ± 0.3	2.30 ± 0.02
Collaborative	4	47.7 ± 0.3	2.44 ± 0.02
Collaborative	5	57.6 ± 0.2	2.54 ± 0.03
Collaborative	6	65.9 ± 0.2	2.62 ± 0.02
Collaborative [1]	6	63.5 ±0.2	2.61 ± 0.02

[1] Stability test: measurements taken following 100 actuation cycles.

4. Discussion

As expected, the force and stroke length comparison testing demonstrated the potential for a string of collaborative PAMs to produce significantly higher output forces than single PAMs, though with some loss of efficiency and significantly less stroke. The 26.1 N maximum force of the five PAM collaborative group is approximately 3.8 times higher than the 6.8 N output of the single PAM. This reduction from a theoretical 5-times increase in force is likely caused by interference between the cables and the outer surface of the PAMs during actuation as well as slight variations between the muscles in length and pre-tension during manufacture. Any mismatch among the PAMs in length or initial tension would cause a difference in deadband effect between a PAM and its collaborators, effectively making it slack and non-productive until it has sufficiently contracted to tension its connection to the actuation cable. This loss of force capability can be addressed in future

designs by investigating the option of routing the cables through the internal lumens of the muscles, removing any potential for interference with the external walls. Differences in PAM initial dimensions or tensioning are best addressed at a process level by ensuring consistent component sizes and manufacturing technique. Even with a slightly reduced force from the theoretically expected output, the proposed design still delivered a significant 380% increase in force output and ability to steer a semi-rigid prototype laser coagulation fetoscope to a small bending radius when compared to the current state-of-the-art. The obtained gain in bending angle was as high as 647%.

It must be said that the absolute stroke length of the collaborative PAMs was significantly reduced relative to the stroke length of the single PAM, fitting the initial hypothesis for the proposed design. The relative stroke was very similar between the prototypes, with the single muscle producing approximately 4.9 times the stroke of the five collaborative prototypes. However, it is important to note that in terms of absolute stroke length, the 10.5 mm produced by the collaborators is a very significant amount for many intrinsically actuated medical device applications. In addition to steerable bending segments, devices such as surgical graspers, scissors, and needle drivers all benefit from very high forces delivered at small stroke lengths. The proposed design therefore offers an interesting alternative to transmitting those high forces from an extrinsic actuation source to the surgical site, making it possible to transform currently unused space along the axis of the device shaft into a high-force intrinsic actuator. This style of embedded low-weight fluidic actuation also provides significant potential to produce devices with similar weight and profile to the existing non-flexible devices used by surgeons, improving their chances of adoption in the marketplace and easing the transition for new surgeons training to use steerable MIS devices.

At full pressurization, the maximum diameter of the PAMs was found to be 2.62 mm, less than the 2.8 mm predicted by the geometry of the materials used in its construction. This difference is expected, as the geometric relationships used to predict maximum diameter do not account for physical constraints such as friction between braid strands sliding relative to one another or the energy required to inflate the elastic bladder. While methods for obtaining a more accurate estimate based on the mechanical properties of the construction materials should be investigated, the simple method proposed in Section 1 has been shown to be useful to provide an upper limit for the size that a PAM can be expected to reach, enabling the design of fluidic actuators for highly constrained spaces with confidence that there will not be interference between components during actuation.

5. Conclusions

This study introduced and evaluated the performance of a novel actuation scheme for intrinsically actuated medical devices. This scheme takes advantage of unused space along the axis of long, thin, minimally invasive surgical devices to embed a series of small diameter fluidic actuators. These collaborate to provide actuation together with very high force relative to the state-of-the-art at absolute stroke lengths which are useful for a wide array of different surgical devices. Though this paper focused on medical robotics applications, the proposed design also has widespread potential to impact the design of soft robotic and fluidic systems. Future work should be conducted to refine the concept, reducing force losses due to interference between moving components, further miniaturizing the proposed design for use in heavily cross-sectionally constrained spaces, and investigating the potential for very long chains of relatively short actuators to actuate lightweight, user-friendly, steerable devices with high driving force requirements.

Author Contributions: Conceptualization, R.L. and E.V.P.; methodology, R.L. and M.O.; software, R.L.; validation, R.L. and E.V.P.; formal analysis, R.L.; investigation, R.L.; writing—original draft preparation, R.L.; writing—review and editing, M.O., J.D. and E.V.P.; supervision, J.D. and E.V.P.; project administration, M.O. and E.V.P.; funding acquisition, J.D. and E.V.P. All authors have read and agreed to the published version of the manuscript.

Funding: This project received funding from the FLEXFET project (3E200384), an internally funded C2 project of KU Leuven.

Data Availability Statement: The data is contained within the article.

Conflicts of Interest: The authors declare no conflicts of interest.

References

1. Tan, A.; Ashrafian, H.; Scott, A.J.; Mason, S.E.; Harling, L.; Athanasiou, T.; Darzi, A. Robotic surgery: Disruptive innovation or unfulfilled promise? A systematic review and meta-analysis of the first 30 years. *Surg. Endosc.* **2016**, *30*, 4330–4352. [CrossRef] [PubMed]
2. Sheetz, K.H.; Claflin, J.; Dimick, J.B. Trends in the Adoption of Robotic Surgery for Common Surgical Procedures. *JAMA Netw. Open* **2020**, *3*, e1918911. [CrossRef] [PubMed]
3. Hu, X.; Chen, A.; Luo, Y.; Zhang, C.; Zhang, E. Steerable catheters for minimally invasive surgery: A review and future directions. *Comput. Assist. Surg.* **2018**, *23*, 21–41. [CrossRef] [PubMed]
4. Ali, A.; Plettenburg, D.H.; Breedveld, P. Steerable Catheters in Cardiology: Classifying Steerability and Assessing Future Challenges. *IEEE Trans. Biomed. Eng.* **2016**, *63*, 679–693. [CrossRef] [PubMed]
5. Gu, X.; Ren, H. A Survey of Transoral Robotic Mechanisms: Distal Dexterity, Variable Stiffness, and Triangulation. *Cyborg Bionic Syst.* **2023**, *4*, 0007. [CrossRef] [PubMed]
6. Duan, J.; Zhang, K.; Qian, K.; Hao, J.; Zhang, Z.; Shi, C. An Operating Stiffness Controller for the Medical Continuum Robot Based on Impedance Control. *Cyborg Bionic Syst.* **2024**, *5*, 0110. [CrossRef] [PubMed]
7. Fan, Y.; Xu, L.; Liu, S.; Li, J.; Xia, J.; Qin, X.; Li, Y.; Gao, T.; Tang, X. The State-of-the-Art and Perspectives of Laser Ablation for Tumor Treatment. *Cyborg Bionic Syst.* **2024**, *5*, 0062. [CrossRef]
8. Garcìa-Garcìa, H.M.; Gogas, B.D.; Serruys, P.W.; Bruining, N. IVUS-based imaging modalities for tissue characterization: similarities and differences. *T Int. J. Cardiovasc. Imaging* **2011**, *27*, 215–224. [CrossRef]
9. Mora, O.C.; Zanne, P.; Zorn, L.; Nageotte, F.; Zulina, N.; Gravelyn, S.; Montgomery, P.; de Mathelin, M.; Dallemagne, B.; Gora, M.J. Steerable OCT catheter for real-time assistance during teleoperated endoscopic treatment of colorectal cancer. *Biomed. Opt. Express* **2020**, *11*, 1231–1243. [CrossRef]
10. Riga, C.; Bicknell, C.; Cheshire, N.; Hamady, M. Initial Clinical Application of a Robotically Steerable Catheter System in Endovascular Aneurysm Repair. *J. Endovasc. Ther.* **2009**, *16*, 149–153. [CrossRef] [PubMed]
11. Sheng, J.; Wang, X.; Dickfeld, T.M.L.; Desai, J.P. Towards the Development of a Steerable and MRI-Compatible Cardiac Catheter for Atrial Fibrillation Treatment. *IEEE Robot. Autom. Lett.* **2018**, *3*, 4038–4045. [CrossRef] [PubMed]
12. Burgner-Kahrs, J.; Rucker, D.C.; Choset, H. Continuum Robots for Medical Applications: A Survey. *IEEE Trans. Robot.* **2015**, *31*, 1261–1280. [CrossRef]
13. Gilbert, H.B.; Rucker, D.C.; Webster III, R.J. Concentric Tube Robots: The State of the Art and Future Directions. In Proceedings of the Robotics Research: The 16th International Symposium ISRR, Singapore, 16–19 December 2016; pp. 253–269.
14. da Veiga, T.; Chandler, J.H.; Lloyd, P.; Pittiglio, G.; Wilkinson, N.J.; Hoshiar, A.K.; Harris, R.A.; Valdastri, P. Challenges of continuum robots in clinical context: A review. *Prog. Biomed. Eng.* **2020**, *2*, 032003. [CrossRef]
15. Ayvali, E.; Liang, C.P.; Ho, M.; Chen, Y.; Desai, J.P. Towards a discretely actuated steerable cannula for diagnostic and therapeutic procedures. *Int. J. Robot. Res.* **2012**, *31*, 588–603. [CrossRef] [PubMed]
16. Carpi, F.; Pappone, C. Stereotaxis Niobe® magnetic navigation system for endocardial catheter ablation and gastrointestinal capsule endoscopy. *Expert Rev. Med. Devices* **2009**, *6*, 487–498. [CrossRef] [PubMed]
17. Devreker, A.; Rosa, B.; Desjardins, A.; Alles, E.; Garcia-Peraza, L.; Maneas, E.; Stoyanov, D.; David, A.; Vercauteren, T.; Deprest, J.; et al. Fluidic actuation for intra-operative in situ imaging. In Proceedings of the 2015 IEEE/RSJ International Conference on Intelligent Robots and Systems (IROS), Hamburg, Germany, 28 September–3 October 2015; Volume 1, pp. 1415–1421.
18. Ahmad, M.A.; Ourak, M.; Wenmakers, D.; Valenzuela, I.; Basurto, D.; Ourselin, S.; Vercauteren, T.; Deprest, J.; Poorten, E.V. Development and validation of a flexible fetoscope for fetoscopic laser coagulation. *Int. J. Comput. Assist. Radiol. Surg.* **2023**, *18*, 1603–1611. [CrossRef] [PubMed]
19. Wang, J.; Gao, D.; Lee, P.S. Recent Progress in Artificial Muscles for Interactive Soft Robotics. *Adv. Mater.* **2021**, *33*. [CrossRef] [PubMed]
20. Andrikopoulos, G.; Nikolakopoulos, G.; Manesis, S. A Survey on applications of Pneumatic Artificial Muscles. In Proceedings of the 2011 19th Mediterranean Conference on Control and Automation (MED), Corfu, Greece, 20–23 June 2011; pp. 1439–1446.
21. Legrand, J.; Ourak, M.; Vander Poorten, E.B. Concentric muscles–Miniature Pneumatic Actuator with Integrated Channel for Surgical Instruments. In Proceedings of the ACTUATOR; International Conference and Exhibition on New Actuator Systems and Applications, Virtual, 17–19 February 2021; pp. 1–4.

22. Lathrop, R.P.; Ourak, M.; Vander Poorten, E. Miniature Pneumatic Artificial Muscles for Use in Surgical Devices. In Proceedings of the ACTUATOR 2022; International Conference and Exhibition on New Actuator Systems and Applications, Mannheim, Germany, 29–30 June 2022.
23. Gaylord, R. Fluid Actuated Motor System and Stroking Device. U.S. Patent 2,844,126, 22 July 1958.